New Journal of Physics
The open access journal at the forefront of physics

Deutsche Physikalische Gesellschaft DPG
IOP Institute of Physics

Published in partnership with: Deutsche Physikalische Gesellschaft and the Institute of Physics

OPEN ACCESS

RECEIVED
25 July 2014

REVISED
2 December 2014

ACCEPTED FOR PUBLICATION
16 January 2015

PUBLISHED
18 February 2015

PAPER

Spectral self-action of THz emission from ionizing two-color laser pulses in gases

Eduardo Cabrera-Granado[1], **Yxing Chen**[2], **Ihar Babushkin**[3,4], **Luc Bergé**[5] **and Stefan Skupin**[6,7,8]

[1] Facultad de Óptica y Optometría, Universidad Complutense de Madrid, 28037, Madrid, Spain
[2] Laboratory for fundamental BioPhotonics, Ecole Polytechnique Fédérale de Lausanne, Switzerland
[3] Humboldt University, Institute of Mathematics, 12489 Berlin, Germany
[4] Institute for Quantum Optics, Leibniz Universität Hannover, Welfengarten 1, 30167 Hannover, Germany
[5] CEA-DAM, DIF, F-91297 Arpajon, France
[6] Max Planck Institute for the Physics of Complex Systems, 01187 Dresden, Germany
[7] Institute of Condensed Matter Theory and Solid State Optics, Abbe Center of Photonics, Friedrich-Schiller-Universität Jena, 07743 Jena, Germany
[8] Univ. Bordeaux — CNRS — CEA, Centre Lasers Intenses et Applications, UMR 5107, 33405 Talence, France

E-mail: ecabrera@ucm.es

Keywords: ultrafast nonlinear optics, photoionization, THz generation, far infrared spectroscopy, multi-color pulses

Abstract

The spectrum of terahertz (THz) emission in gases via ionizing two-color femtosecond pulses is analyzed by means of a semi-analytic model and numerical simulations in 1D, 2D and 3D geometries taking into account propagation effects of both pump and THz fields. We show that produced THz signals interact with free electron trajectories and thus significantly influence further THz generation upon propagation, i.e., make the process inherently nonlocal. This self-action contributes to the observed strong spectral broadening of the generated THz field. We show that diffraction of the generated THz radiation is the limiting factor for the co-propagating low frequency amplitudes and thus for the self-action mechanism in 2D and 3D geometries.

1. Introduction

Research on intense terahertz (THz) electromagnetic sources has received an increasing amount of attention owing to their numerous applications, for example, in time-domain spectroscopy, biomedical imaging or security screening [1]. Among the various techniques employed to generate THz radiation, focusing intense two-color femtosecond pulses in air or noble gases provides interesting features like the absence of material damage, large generated bandwidths (up to ∼100 THz) and high amplitudes of the emitted THz pulses (>100 MV m^{-1}) [2]. First reported by Cook *et al* [3], THz emission from intense two-color pulses was initially attributed to optical rectification via third-order nonlinearity. However, it was shown later that the plasma built-up by tunneling photoionization is necessary to explain the high amplitudes of the THz field [4–6], and a quasi-dc plasma current generated by the temporally asymmetric two-color field is responsible for THz emission [7, 8]. Plasma oscillations leading to strong THz radiation were also reported for single-color pump pulses with few-cycle duration or at higher intensities [9, 10].

Apart from energy scaling [11] and polarization control [12], tailoring the shape of the broadband radiated THz pulse is one of the current goals with respect to applications. In the case of two-color filaments in air it was already demonstrated experimentally that the geometry of the plasma channels and the initial carrier envelope phase of the laser pulse can be used to control the THz waveform [13, 14]. Recently, controlling THz generation in gases by more involved spectral engineering of the IR pump pulse was also suggested, i.e., by modifying the temporal positions of the electric field maxima resp. ionization events [15].

One of the main challenges on the route towards THz spectral control is to understand the influence of the complicated nonlinear propagation dynamics of the electromagnetic radiation. It is known that ionizing femtosecond laser pulses undergo strong spatiotemporal modifications during propagation, and that these

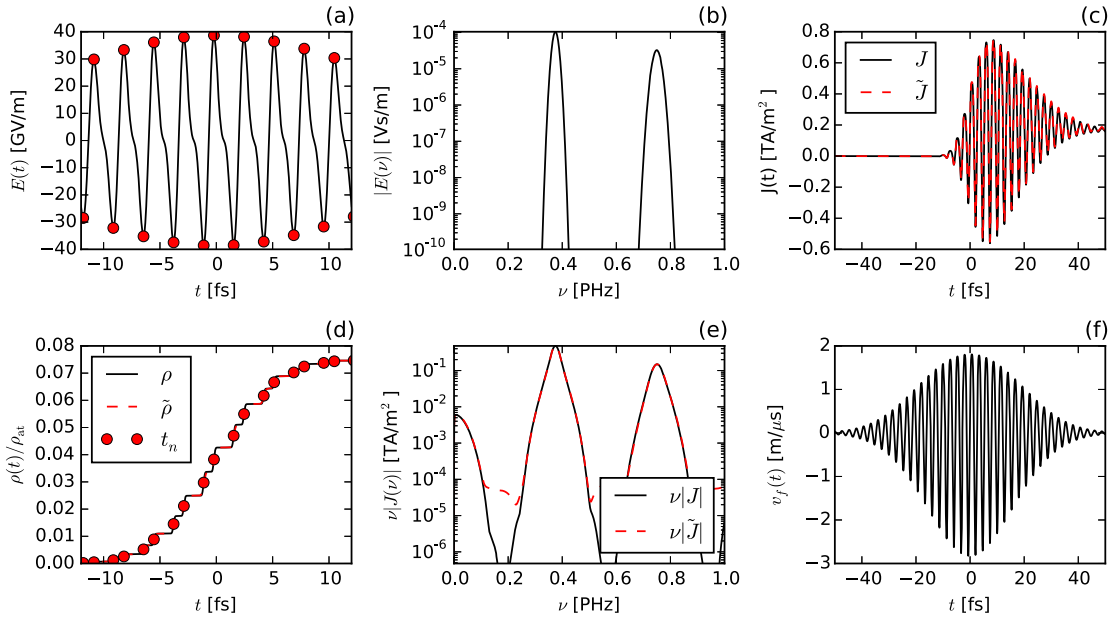

Figure 1. (a) Exemplary two-color electric field $E(t)$ (see equation (7) and text below for details); (b) corresponding spectrum; (c) current density $J(t)$ and (d) plasma density $\rho(t)$ given by equations (3) and (1). (e) The resulting spectrum of the secondary electric field $E_J \propto \nu J$ (see equation (6)), and (f) the free electron velocity v_f (see equation (5)). Results of our semi-analytic model equations (2) respectively (4), $\tilde{\rho}(t)$ and $\tilde{J}(t)$, are marked as red dashed lines in (c), (d), and (e), showing excellent agreement. Red dots in (a) and (d) indicate the temporal positions t_n of the ionization events.

propagation effects have a tremendous impact on the emitted THz fields [16]. Moreover, shortly after the onset of THz generation the gas atoms or molecules and ionized electrons are exposed to the co-propagating low-frequency field as well. In particular, because asymmetrically ionized gases were already successfully used for remote detection of THz fields through coherent manipulation of the ionized electron drift velocity and subsequent collision-induced fluorescence emission [17], we can expect to find a self-action mechanism of already generated THz radiation on the THz generation itself.

2. Model

In the present work we will shed light onto the pulse propagation effects in the plasma, and the interaction of the generated terahertz field with the ionized medium. Our starting point is a semi-analytic model developed in [15] based on the local current (LC) approximation, i.e., considering a small volume of gas irradiated by the ionizing field. Let us assume that the free electron density is governed by

$$\partial_t \rho(t) = W_{\mathrm{ST}}(E)\Big[\rho_{at} - \rho(t)\Big], \tag{1}$$

where $W_{\mathrm{ST}}(E)$ is a field-dependent tunneling ionization rate [5], leading to a stepwise increase of $\rho(t)$ in time (see figure 1(d)). The nth ionization event with amplitude $\delta\rho_n$ and temporal shape $H_n(t)$ corresponds to a maximum of the incoming field at time t_n. Because all ionization events share a similar shape [9], we can simplify $H_n(t) \simeq H(t - t_n) = \Big\{1 + \mathrm{erf}\left[(t - t_n)/\tau\right]\Big\}\Big/2$, with characteristic temporal width $\tau = 0.2$ fs. This value was found to fit well the "typical" duration of an ionization event (see appendix A.1. of [15]). The events are well separated in time, so we can give a semi-analytic expression for $\rho(t)$ by summing up all contributions

$$\rho(t) \approx \tilde{\rho}(t) = \sum_n \delta\rho_n H\Big(t - t_n\Big). \tag{2}$$

For a given electric field amplitude $E(t)$, the $\delta\rho_n$ and t_n can be extracted from the numerical solution of equation (1).

If we assume zero velocity for newly born electrons and neglect ponderomotive forces, the equation for the plasma current density reads

[9] Provided that pump pulses are multi-cycle, and $\rho(t) \ll \rho_{at}$.

$$\frac{\mathrm{d}J(t)}{\mathrm{d}t} + \gamma J(t) = \frac{q^2}{m}\rho(t)E(t). \tag{3}$$

Here, γ is a phenomenological electron–ion collision rate, and q, m represent electron charge and mass, respectively. We choose $\gamma = 7.7\ \mathrm{ps}^{-1}$ throughout this paper, a value compatible with usual estimates [18] for free electron densities and velocities of the order of $10^{18} - 10^{19}\ \mathrm{cm}^{-3}$ and $\sim 10^6\ \mathrm{m\,s}^{-1}$, respectively. Finally, plugging the above approximation $\tilde{\rho}(t)$ (equation (2)) for the plasma density $\rho(t)$ into equation (3) yields a semi-analytic expression for the current

$$J(t) \approx \tilde{J}(t) = \sum_n q\delta\rho_n H\left(t - t_n\right)\left[v_\mathrm{f}(t) - \mathrm{e}^{\gamma\left(t_n - t\right)}v_\mathrm{f}\left(t_n\right)\right]. \tag{4}$$

Here, the expression

$$v_f(t) = \frac{q}{m}\int_{-\infty}^{t} E(\tau)\mathrm{e}^{\gamma(\tau - t)}\mathrm{d}\tau \tag{5}$$

can be interpreted as the free electron velocity. Figure 1 confirms excellent agreement between numerical evaluation of equations (1), (3) and our semi-analytic expression equations (2), (4) for both plasma and current density. In fact, throughout the whole analysis presented in this paper we found that the approximations $\rho(t) \approx \tilde{\rho}(t)$ and $J(t) \approx \tilde{J}(t)$ are always close to equality.

The emitted secondary electric field due to the plasma current can be calculated in frequency domain as

$$E_J(\omega) = g\omega J(\omega), \tag{6}$$

where g is a constant [19]. In figure 1(e) we show the spectrum of the secondary radiation according to equation (6) for a representative (linearly polarized) two-color pump field

$$E(t) = E_0\left[\mathrm{e}^{-\frac{t^2}{t_p^2}}\cos(\omega t) + r\mathrm{e}^{-\frac{t^2}{2t_p^2}}\cos(2\omega t + \phi)\right], \tag{7}$$

where $E_0 = 31\ \mathrm{GV\,m}^{-1}$, $t_p = 24$ fs, $\omega = 2\pi\nu$ with $\nu = 375$ THz, and the ratio $r = 0.44$ between the fundamental and second-harmonic. The relative phase between both fields has been set to $\phi = \pi/2$, to ensure optimum conditions for THz generation [5]. Throughout this paper all quantities, including spectra, are expressed in physical units.

3. THz spectral self-action

It is a reasonable assumption that an additional small low frequency field will co-propagate with the pump pulse shortly after the onset of THz generation. Thus, let us now investigate the impact of such a field on the secondary radiation spectrum. To this end, we add a third component centered at 50 THz, ~15 fs duration and with only 2 % the amplitude of the fundamental IR frequency to the two-color field equation (7) (see figure 2(a)). As can be seen in figure 2(d), the low-frequency spectral shape of the secondary radiation changes noticeably compared to figure 1(e), a peak around the frequency of the new pump component now dominates the low frequency range. This simple example already indicates that generated THz fields have an important impact on the subsequent THz generation process, and thus produce a self-action. In other words, the THz generation process from ionizing two-color pulses is nonlinear, and the nonlinearity is significantly nonlocal in propagation direction of the pump laser.

Before performing any further analysis, we want to investigate the influence of the phase angle ϕ between the fundamental and second-harmonic field. The secondary radiation spectra shown in figures 1(e) and 2(d) are obtained for $\phi = \pi/2$. It is well known that for a pure two-color driving field this value ensures maximum THz yield $\propto \int_0^{100\ \mathrm{THz}} \nu^2 |J(\nu)|^2 \mathrm{d}\nu$, as recalled by the dashed line in figure 2(c). With the small THz component present in the driving field, this THz yield increases considerably for almost all values of ϕ (see solid curve in figure 2(c)), and the frequency of the maximum spectral density increases as well (see figure 2(f)). The jump in figure 2(f) around $\phi = 3\pi/2$ is linked to the exceptionally low THz yield in this parameter range (see figure 2(c)). Thus, we can state that the additional THz pump field component, even with a small amplitude, dominates the low frequency spectral shape of the secondary emission for almost all values of ϕ. We also found that the phase angle of the THz pump component itself is of minor influence (not shown), which is probably due to the much longer duration of the THz optical-cycle.

We can use the semi-analytic approximate expression for the plasma current $\tilde{J}(t)$, equation (4), to gain further insight into the THz spectral self-action mechanism. To this end, we rewrite the secondary field as the sum of two contributions,

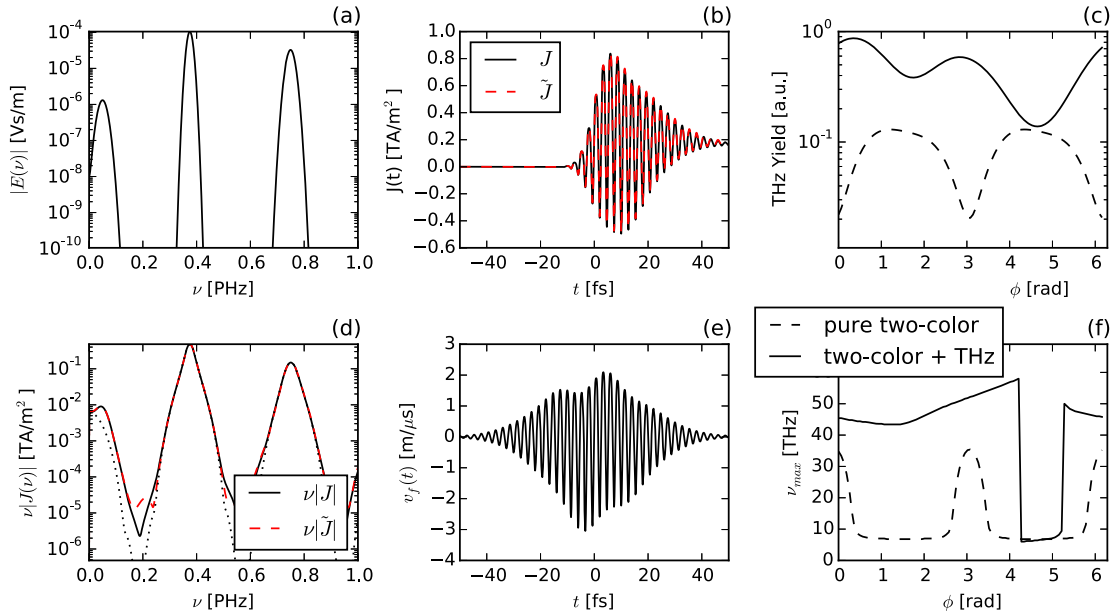

Figure 2. (a) Spectrum of the exemplary pump field with THz component centered at 50 THz (see text for details); (b) corresponding current density $J(t)$; (c) yield of secondary radiation below 100 THz for the pump field in (a) (solid curve) and the pure two-color field of figure 1 (dashed curve) versus phase angle ϕ. (d) Spectrum of the secondary electric field $E_J \propto \nu J$; the spectrum of figure 1(e) is recalled by the black dotted curve. (e) Free electron velocity v_f for the pump field in (a). (f) Position of the maximum spectral density of secondary radiation below 100 THz, same line coding as in (c). Results of our semi-analytic model ($\tilde{J}$, see equation (4)) are marked as red dashed lines in (b) and (d), again showing excellent agreement.

$$E_J(\omega) = g\omega J(\omega) \approx g\omega\tilde{J}(\omega) = g\,[A(\omega) - B(\omega)], \tag{8}$$

where

$$A(\omega) = q\omega\mathrm{FT}\left[v_f(t)\sum_n \delta\rho_n H\left(t - t_n\right)\right], \tag{9}$$

$$B(\omega) = q\omega\mathrm{FT}\left[\sum_n \delta\rho_n H\left(t - t_n\right) e^{\gamma\left(t_n - t\right)} v_f\left(t_n\right)\right]. \tag{10}$$

Here, FT[ ] denotes the Fourier transform. Interestingly, for a two-color pump field without any low-frequency components, in the optimum configuration ($\phi = \pi/2$, see figure 1), the secondary radiation $E_J(\nu)$ below 100 THz is determined solely by $B(\nu)$ [15]. This is confirmed by figure 3(a), where the secondary radiation $E_J(\nu) \propto \nu J(\nu)$ is separated into $A(\nu)$ and $B(\nu)$ according to equations (9) and (10). Once low-frequency components are present, $A(\nu)$ starts to contribute as well through the free electron velocity $v_f(t)$. Figure 3(b) illustrates the impact of $A(\nu)$ and $B(\nu)$ for the pump field configuration of figure 2 and reveals the THz spectral self-action mechanism: the term $A(\nu)$ describes the impact of the electric field on the plasma current, because $A(\nu)$ contains $v_f(t)$[10]. In fact, the change in the free electron velocity $v_f(t)$ is clearly visible when comparing figure 1(f) with figure 2(e). As we can observe from figure 3(c), the low frequency component of $E(t)$ resp. $v_f(t)$ can significantly alter the free electron trajectory and thus the secondary radiation spectrum. From the mathematical structure of equation (9) we can infer that $A(\nu)$ yields a similar spectrum to the pump field $E(\nu)$ but broader due to the convolution of FT$[v_f(t)]$ with FT$[H(t)]$ in the Fourier domain, which is confirmed by figure 3. Because the secondary radiation is co-propagating with the pump field, a spectral self-action occurs and we expect a THz spectral broadening upon propagation.

4. Simulations

To confirm our previous hypothesis of THz spectral self-action, we present several numerical simulations in various geometries ranging from 1D (hollow fiber waveguide) to 3D (bulk material, gas) configurations. In a first attempt, we propagate the two-color field equation (7) [11] over 400 μm in argon gas by means of the 1D-

[10] In contrast to $B(\nu)$, which contains $v_f(t_n)$ only.

[11] In all simulations no THz component is present at the beginning of the simulation.

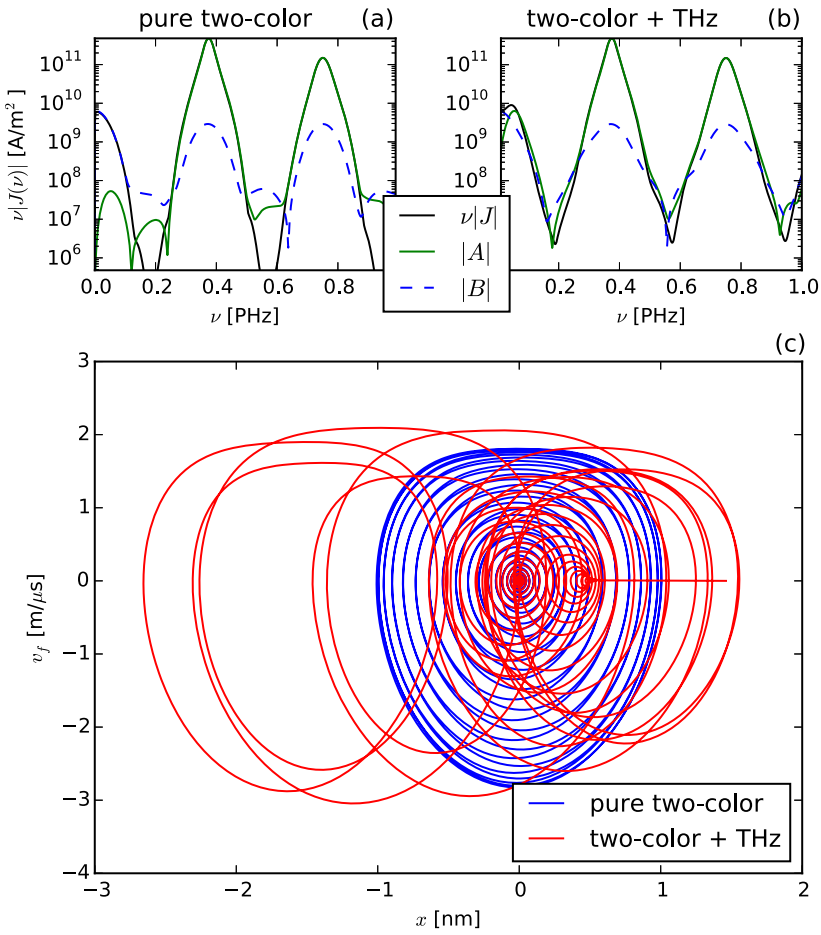

Figure 3. Spectrum of secondary radiation $E_J(\nu) \propto \nu J(\nu)$ (black solid line) for (a) a pure two-color pump pulse (see figure 1) and (b) with an additional low amplitude component centered around 50 THz (see figure 2). Our semi-analytic model, equations (9) and (10), allows a decomposition into $A(\nu)$ (green solid lines) and $B(\nu)$ (blue dashed lines). The term $A(\nu)$, which contains the impact of the electric field on the plasma current via the free electron velocity $v_f(t)$, is clearly responsible for the modification of the secondary radiation in THz spectral range. In (c) the phase-space representation of the motion of a free electron born at $t = -\infty$ is shown for both pump field configurations. The dramatic impact of the THz component in the electron trajectory is clearly visible.

finite-difference-time-domain (1D-FDTD) algorithm [20]. Nonlinear generalization of the FDTD algorithm offers the possibility to simulate Maxwell's equations without further approximations [21]. Linear dispersion of argon is included via the refractive index $n(\omega)$ given in [22]. The plasma density $\rho(t)$ obeys equation (1), and the resulting plasma current $J(t)$ is accounted for via equation (3). Figure 4(a,d,g) shows the spectrum of the propagated field $E(\nu)$ at three different distances. We can clearly see that the low frequency spectrum (red part of the curve) broadens up to frequencies well above 100 THz during propagation in the medium, in agreement with our previous expectations. Solid black lines in figure 4(b,e,h) show the corresponding local secondary emission $E_J(\nu) \propto \nu J(\nu)$. Interestingly, the maximum of the low frequency secondary emission spectrum shifts toward larger frequencies with increasing propagation distance, an effect already reported in [16, 23].

In order to further corroborate the THz spectral feedback mechanism, hypothetical local secondary emission spectra computed from a modified pump field with the low frequency part (<200 THz) suppressed are plotted in figure 4(b,e,h) for comparison (dashed lines). Obviously, local spectra generated by these artificially modified pump fields are less broad than the original spectra, in particular towards larger propagation distances where strong THz spectral broadening takes place. By using the semi-analytic model developed above, we can decompose the local secondary emission $\nu J(\nu)$ into the contributions of $A(\nu)$ and $B(\nu)$. As predicted above and confirmed by figure 4(c,f,i), the low frequency part of $A(\nu)$ is determined by the low frequency part of the driving field E, and thus responsible for the THz spectral feedback mechanism. In contrast, we report minor changes only in $B(\nu)$ when the low frequency part of the pump field is suppressed (not shown).

Thus, in the present propagation regime with relatively narrow IR pump spectra, the THz spectral feedback mechanism is a key player with a strong impact on the emitted secondary radiation. At larger propagation distances, spectral broadening and shifting of the two-color pump pulse itself may become the dominant effect determining the local secondary emission THz spectra. In fact, it is important to keep in mind that the THz

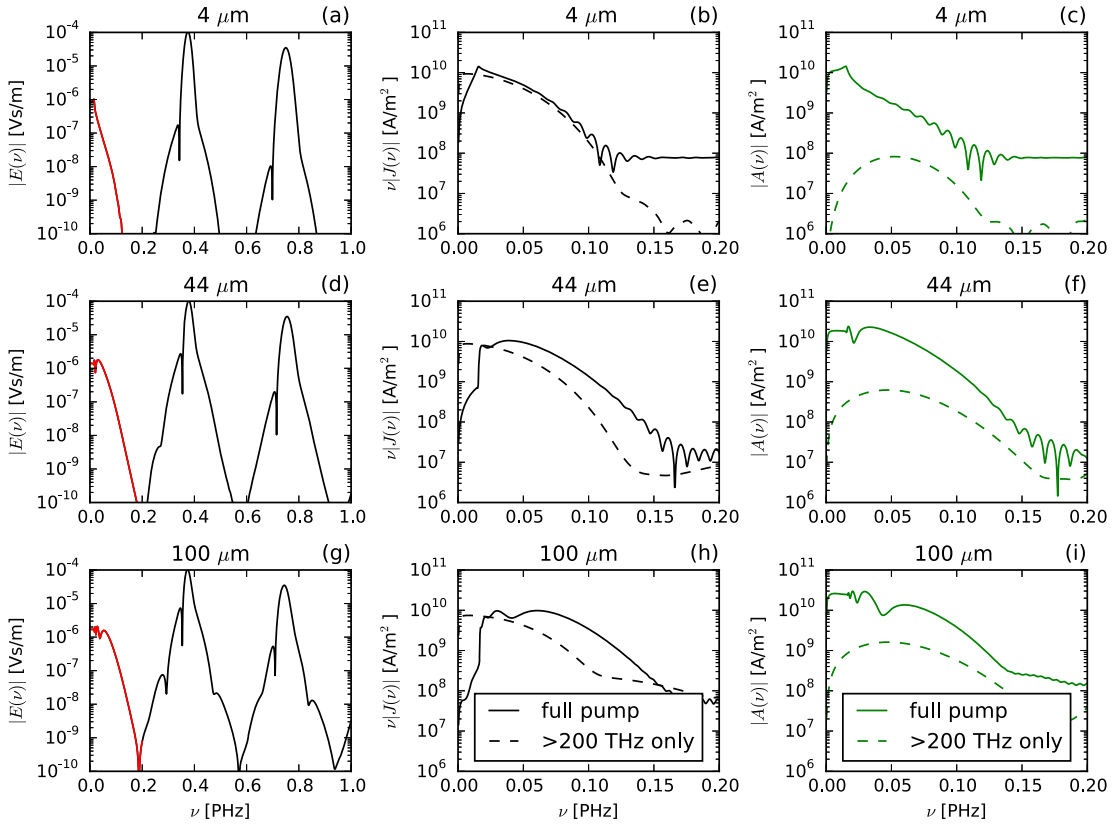

Figure 4. (a,d,g) Recorded electric field spectrum from 1D-FDTD simulations at indicated propagation distances, with the low frequency part marked in red. (b,e,h) Corresponding local secondary emission $E_J(\nu) \propto \nu J(\nu)$ in the range below 200 THz (solid black lines). The dashed lines show the same quantity computed from a modified pump field with the low frequency part (<200 THz) suppressed. (c,f,i) The contribution $A(\nu)$ to the local secondary emission according to equation (9) computed with (solid green lines) and without (dashed green lines) low frequency part of the pump.

spectral feedback mechanism reported here is an additional effect, and other propagation effects modifying the THz spectra are present as well [7, 16].

In 1D geometries investigated so far, high pump intensities are maintained over extended propagation ranges due to the absence of transverse diffraction, and thus nonlinear effects are stronger than in 2D or even 3D geometries. To address the role of diffraction, 2D-FDTD simulations have been performed, employing a focused ($f = 330$ μm) beam with initial width $w_0 = 30.2$ μm. Results are shown in figure 5. The initial fundamental amplitude was taken as 11.5 GV m^{-1}, in order to reach 47 GV m^{-1} peak amplitude at focus. Other parameters are kept as in the 1D simulations (see equation (7)). The interaction of the generated THz field with the newly born free electrons as the field propagates through the medium is expected to be weaker than in the 1D configuration, because the low frequency part of the field strongly diffracts and leaves the plasma channel. Nevertheless, as the field propagates, the maximum of the secondary radiation spectrum in THz range shifts towards higher frequencies until the focal point is reached (see figure 5(a,c,e)). Dashed curves in figure 5(b,d,f) show on-axis local secondary emission spectra $E_J(\nu) \propto \nu J(\nu)$ computed from pump fields with low frequency range (<200 THz) suppressed. Local spectra generated near the focus by these artificially modified pump fields are shifted by more than 10 THz towards lower frequencies compared to the original local spectra plotted in black solid lines. We note that in simulations reaching higher peak electric field amplitudes >50 GV m^{-1} at focus, the THz self-action can be more pronounced. However, our model accounting for single ionization only becomes questionable in this strong-field regime [24], and we do not discuss this regime in the present work. In contrast, simulations with reduced fundamental peak amplitude reaching only 37 GV m^{-1} at focus (not shown) feature no THz spectral self-action at all, simply because the on-axis THz field amplitude remains one order of magnitude lower. The rapid oscillations visible in the spectra in figure 5(b,d,f) are numerical artefacts due to the limited propagation range (i.e., temporal extent of the recorded time series) in our 2D simulations.

In general, THz self-action in 2D geometry is less pronounced than in the former 1D case. Moreover, from the focal point onward, figure 5(d,f) shows that the maximum of the secondary field spectrum remains fixed around $\nu \sim 50$ THz. These features can be readily explained by the strong diffraction of the THz field beyond the focus, which prevents the low frequency field from driving the free electrons produced in the plasma channel,

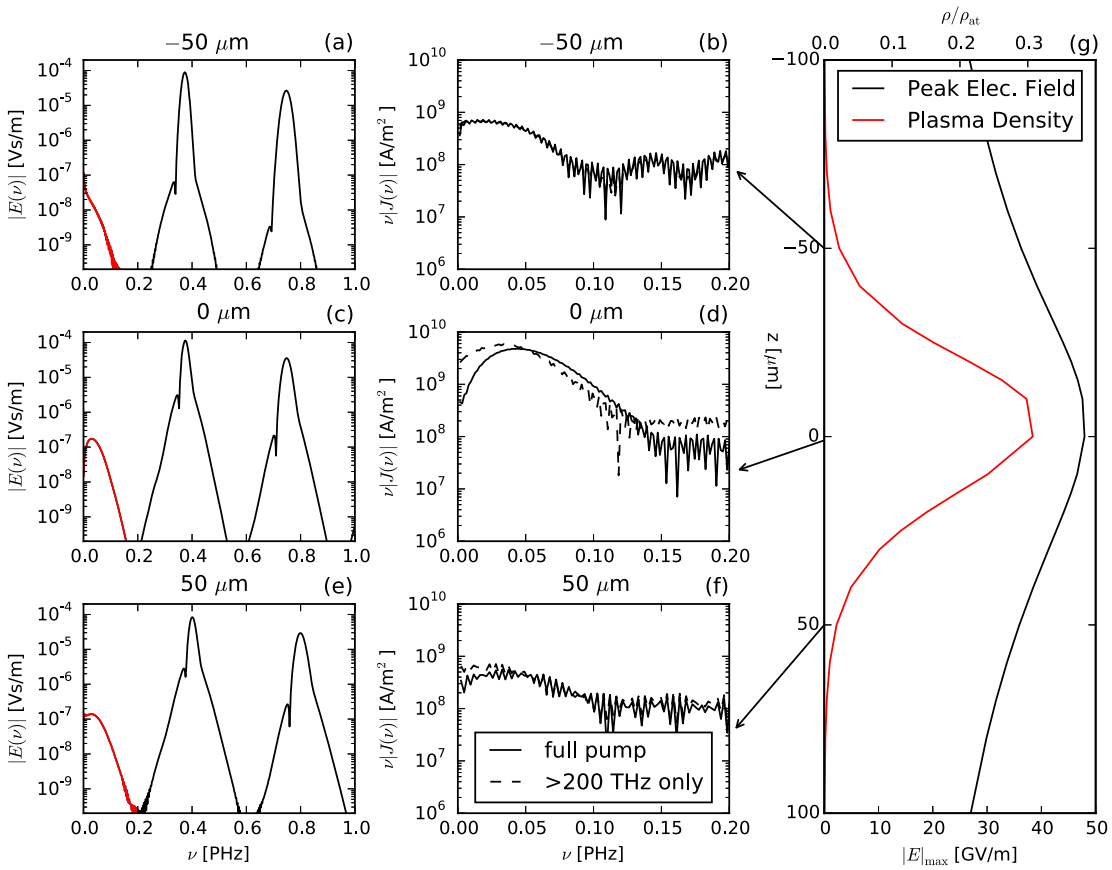

Figure 5. (a,c,e) Recorded on-axis electric field spectrum from 2D-FDTD simulations at indicated propagation distances, with the low frequency part marked in red. (b,d,f) Corresponding on-axis local secondary emission $E_J(\nu) \propto \nu J(\nu)$ in the range below 200 THz (solid black lines). The dashed lines show the same quantity computed from a modified pump field with the low frequency part (<200 THz) suppressed. (g) Peak electric field amplitude and plasma density versus propagation distance z, with $z = 0$ denoting the focal point.

and therefore arrests the THz spectral self-action mechanism. In figure 6 the action of diffraction on the different spectral components of the electric field at 30 μm after the geometrical focus is visualized. One can clearly see that diffraction delocalizes the THz radiation much more strongly than the IR and visible light, which rapidly decreases the on-axis THz field strength. Thus, diffraction is a dominant mechanism in determining the final bandwidth of the secondary emission.

The strong impact of diffraction on the THz spectral self-action mechanism observed in the 2D simulations raises the natural question of what happens in a full 3D configuration. In many relevant cases the peak electric field amplitude is limited by so-called intensity clamping [25], and THz fields will undergo strong diffraction. Thus, it is *a priori* not obvious whether THz field amplitudes inside the interaction volume are strong enough to observe THz spectral self-action or not. In order to check this point, we resort to full 3D simulation data of two-color femtosecond filamentation published earlier in [7]. In this work, collimated two-color pulses were launched in an argon atmosphere at ambient pressure in order to produce filaments at clamping intensity over several tens of centimeters. Simulations were performed using the unidirectional pulse propagation model [16, 26]. Strong broadband THz emission was observed for pump pulses with a peak power of 0.3 TW, i.e., 30 times the critical power for self-focusing (see original article for details). In figure 7, we present the analysis of one of the 3D simulation data (20 fs Gaussian pulse, red curves in figure 3 from [7]), in complete analogy to figure 5. To this end, we re-processed the raw data of the 3D simulation to extract the on-axis electric field as a function of time and propagation distance. Then, figure 7 was produced by using these electric field data. In particular, the dashed lines in figure 7(b,d,f) were obtained by calculating the local current from the extracted electric fields with low frequency range (<200 THz) suppressed. Figure 7 clearly confirms that (i) sufficiently high THz amplitudes for THz spectral self-action can be generated in 3D geometry and (ii) THz spectral self-action modifies the spectrum of THz emission from two-color femtosecond filaments.

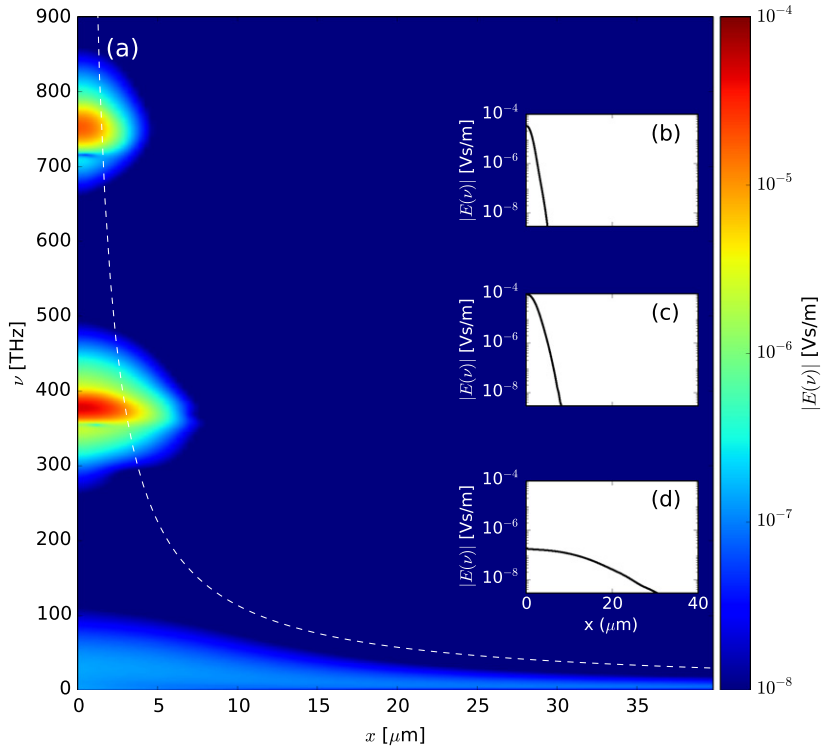

Figure 6. (a) Spatially resolved electric field spectrum (log scale) of the propagating beam in 2D-FDTD simulations obtained at 30 μm after the geometrical focus. Because of symmetry we show the positive transverse x-axis only. Line-outs of spatial profiles versus coordinate x for frequencies $\nu = 375$ THz, $\nu = 750$ THz and $\nu = 30$ THz are shown in panels (b), (c) and (d), respectively. The white dashed line in (a) serves as an eye-guide and shows the expected beam width $w(\nu) \propto 1/\nu$ for a perfect Gaussian beam for all frequencies. Beam parameters are the same as in figure 5.

5. Conclusions

In conclusion, we have investigated THz emission via ionizing two-color femtosecond pulses and revealed a THz spectral self-action mechanism. This mechanism stems from the interaction of the already generated THz field with the subsequent free electron dynamics in the plasma channel and contributes to the strong THz spectral broadening frequently observed in experiments and simulations. Direct simulations in 1D, 2D and 3D geometries support our semi-analytic model and show that diffraction of the THz radiation plays an important role in determining the final bandwidth of the secondary emission by limiting the interaction length of the low-frequency field with the plasma. We believe that our findings may have implications beyond the generation of broadband THz radiation, namely, on the interpretation of recent experiments on high harmonic generation with two-color pulses [27]. Because of the similar pump pulse configuration, generated THz radiation may alter electron trajectories on time scales relevant to the high harmonic generation process as well (see figure 3(c)).

Acknowledgments

Numerical simulations were performed using high performance computing resources at Rechenzentrum Garching (RZG). We acknowledge the development of IPython [28]. ECG and SS acknowledge support by the project PRI-AIBDE-2011-0902 resp. DAAD-PPP-54367872. IB acknowledges the support of DFG (SFB-910).

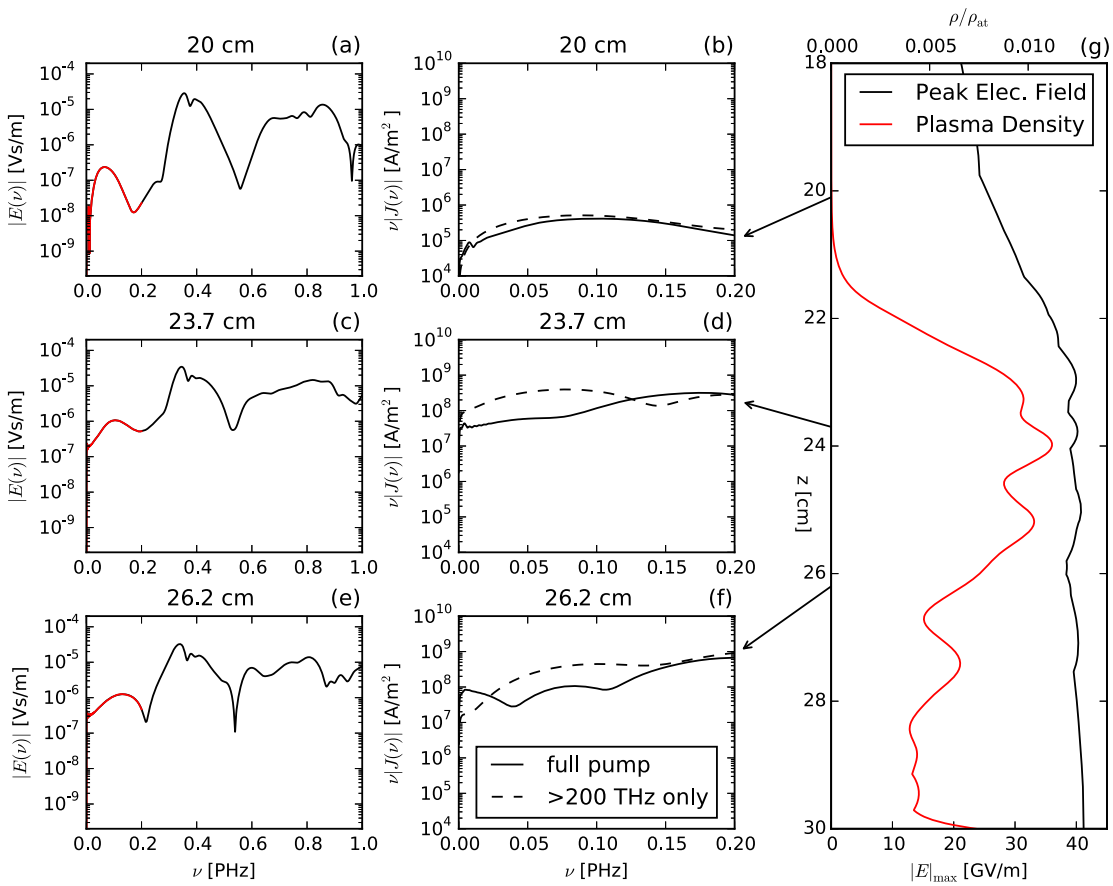

Figure 7. (a,c,e) Recorded on-axis electric field spectrum from 3D unidirectional pulse propagation simulations [7] at indicated propagation distances, with the low frequency part marked in red. (b,d,f) Corresponding on-axis local secondary emission $E_J(\nu) \propto \nu J(\nu)$ in the range below 200 THz (solid black lines). The dashed lines show the same quantity computed from a modified pump field with the low frequency part (<200 THz) suppressed. (g) Peak electric field amplitude and plasma density versus propagation distance z.

References

[1] Tonouchi M 2007 *Nat. Photonics* **1** 97
[2] Kim K Y, Glownia J H, Taylor A J and Rodriguez G 2012 *IEEE J. Quant. Electron* **48** 797
[3] Cook D J and Hochstrasser R M 2000 *Opt. Lett.* **25** 1210
[4] Kress M, Löffler T, Eden S, Thomson M and Roskos H G 2004 *Opt. Lett.* **29** 1120
[5] Thomson M, Kress M, Löffler T and Roskos H 2007 *Laser Photonics Rev.* **1** 349
[6] Kim K Y, Taylor A J, Glownia J H and Rodriguez G 2008 *Nat. Photonics* **2** 605
[7] Bergé L, Skupin S, Köhler C, Babushkin I and Herrmann J 2013 *Phys. Rev. Lett.* **110** 073901
[8] Borodin A V, Panov N A, Kosareva O G, Andreeva V A, Esaulkov M N, Makarov V A, Shkurinov A P, Chin S L and Zhang X C 2013 *Opt. Lett.* **38** 1906
[9] Chen M, Pukhov A, Peng X Y and Willi O 2008 *Phys. Rev.* E **78** 046406
[10] Wang W M, Kawata S, Sheng Z M, Li Y T, Chen L M, Qian L J and Zhang J 2011 *Opt. Lett.* **36** 2608
[11] Oh T I, You Y S, Jhajj N, Rosenthal E W, Milchberg H M and Kim K 2013 *New J. Phys.* **15** 075002
[12] Wen H and Lindenberg A M 2009 *Phys. Rev. Lett.* **103** 023902
[13] Manceau J M, Averchi A, Bonaretti F, Faccio D, Di Trapani P, Couairon A and Tzortzakis S 2009 *Opt. Lett.* **34** 2165
[14] Bai Y, Song L, Xu R, Li C, Liu P, Zeng Z, Zhang Z, Lu H, Li R and Xu Z 2012 *Phys. Rev. Lett.* **108** 255004
[15] Babushkin I, Skupin S, Husakou A, Köhler C, Cabrera-Granado E, Bergé L and Herrmann J 2011 *New J. Phys.* **13** 123029
[16] Babushkin I, Kuehn W, Köhler C, Skupin S, Bergé L, Reimann K, Woerner M, Herrmann J and Elsaesser T 2010 *Phys. Rev. Lett.* **105** 053903
[17] Liu J, Dai J, Chin S L and Zhang X C 2010 *Nat. Photonics* **4** 627
[18] Huba J D (ed) 2013 *NRL Plasma Formulary* (Washington, DC: U.S. GPO)
[19] Jefimenko O D 1966 *Electricity and Magnetism: An Introduction to the Theory of Electric and Magnetic Fields* (New York: Appleton-Century-Crofts)
[20] Taflove A 1995 *Computational Electrodynamics: The Finite-Difference Time-Domain Method* (Norwood: Artech House)
[21] Etrich C, Iliew R, Staliunas K, Lederer F and Egorov O A 2011 *Phys. Rev.* A **84** 021808
[22] Dalgarno A and Kingston A E 1960 *Proc. R. Soc. London* A **259** 424
[23] Babushkin I, Skupin S and Herrmann J 2010 *Opt. Express* **18** 9658
[24] Geltman S 1996 *Phys. Rev.* A **54** 2489
[25] Bergé L, Skupin S, Nuter R, Kasparian J and Wolf J P 2007 *Rep. Prog. Phys.* **70** 1633
[26] Kolesik M and Moloney J V 2004 *Phys. Rev.* E **70** 036604
[27] Brugnera L, Hoffmann D J, Siegel T, Frank F, Zaïr A, Tisch J W G and Marangos J P 2011 *Phys. Rev. Lett.* **107** 153902
[28] Pérez F and Granger B E 2007 *Comput. Sci. Eng.* **9** 21